Canadian Journal of Remote Sensing, 00:1–20, 2016

ISSN: 0703-8992 print / 1712-7971 online
DOI: 10.1080/07038992.2016.1196582

Taylor & Francis
Taylor & Francis Group

Imputation of Individual Longleaf Pine (*Pinus palustris* Mill.) Tree Attributes from Field and LiDAR Data

Carlos A. Silva[1,*], Andrew T. Hudak[2], Lee A. Vierling[1], E. Louise Loudermilk[3], Joseph J. O'Brien[3], J. Kevin Hiers[4], Steve B. Jack[5], Carlos Gonzalez-Benecke[6], Heezin Lee[7], Michael J. Falkowski[8], and Anahita Khosravipour[9]

[1]*Department of Forest, Rangeland, and Fire Sciences, College of Natural Resources, University of Idaho, Moscow, ID 83843, USA*
[2]*USDA Forest Service, Rocky Mountain Research Station, Moscow, ID 83843, USA*
[3]*USDA Forest Service, Southern Research Station, Athens, GA 30602, USA*
[4]*Office of Environmental Stewardship, University of the South, Sewanee, TN 37383, USA*
[5]*Joseph W. Jones Ecological Research Center, 3988 Jones Center Drive, Newton, GA 39870-8522, USA*
[6]*Department of Forest Engineering, Resources and Management, Oregon State University, Corvallis, OR, 97331, USA*
[7]*Department of Earth and Planetary Science, University of California, Berkeley, CA, 94720, USA*
[8]*Department of Ecosystem Science and Sustainability, Colorado State University, Fort Collins, CO 80523, USA*
[9]*Department of Natural Resources, University of Twente, 7500 AE, Enschede, The Netherlands*

Abstract. Light Detection and Ranging (LiDAR) has demonstrated potential for forest inventory at the individual-tree level. The aim in this study was to predict individual-tree height (Ht; m), basal area (BA; m^2), and stem volume (V; m^3) attributes, imputing Random Forest *k*-nearest neighbor (RF *k*-NN) and individual-tree-level-based metrics extracted from a LiDAR-derived canopy height model (CHM) in a longleaf pine (*Pinus palustris* Mill.) forest in southwestern Georgia, United States. We developed a new framework for modeling tree-level forest attributes that comprise 3 steps: (*i*) individual tree detection, crown delineation, and tree-level-based metrics computation from LiDAR-derived CHM; (*ii*) automatic matching of LiDAR-derived trees and field-based trees for a regression modeling step using a novel algorithm; and (*iii*) RF *k*-NN imputation modeling for estimating tree-level Ht, BA, and V and subsequent summarization of these metrics at the plot and stand levels. RMSDs for tree-level Ht, BA, and V were 2.96%, 58.62%, and 8.19%, respectively. Although BA estimation accuracy was poor because of the longleaf pine growth habitat, individual-tree locations, Ht, and V were estimated with high accuracy, especially in low-canopy-cover conditions. Future efforts based on the findings could help improve the estimation accuracy of individual-tree-level attributes such as BA.

Résumé. Le lidar a démontré son potentiel pour l'inventaire forestier à l'échelle de l'arbre. Le but de cette étude était de prédire la hauteur individuelle des arbres (Ht; m), la surface terrière (BA; m^2), et le volume des tiges (V; m^3) en utilisant une imputation basée sur la méthode des forêts aléatoires et des *k* plus proches voisins (RF *k*-NN; *Random Forest k-nearest neighbor*) et de mesures à l'échelle de l'arbre extraites à partir d'un modèle de la hauteur de la canopée (MHC) dérivés du lidar dans une forêt de pins des marais (*Pinus palustris* Mill.) dans le sud-ouest de la Géorgie, aux États-Unis. Nous avons développé un nouveau cadre pour la modélisation des attributs forestiers à l'échelle de l'arbre composé de trois étapes: (*i*) la détection des arbres individuels, la délimitation des couronnes et le calcul de paramètres à l'échelle de l'arbre à partir de modèles MHC obtenus à partir du lidar; (*ii*) la mise en correspondance automatique entre les arbres obtenus à partir du lidar et les arbres observés sur le terrain pour une étape de modélisation de régression en utilisant un nouvel algorithme; et (*iii*) l'imputation par modélisation en utilisant RF *k*-NN pour estimer la Ht, la BA, et le V à l'échelle de l'arbre et la synthèse ultérieure de ces mesures à l'échelle de la parcelle et du peuplement. Les REQM pour la Ht, la BA, et le V à l'échelle de l'arbre étaient de 2,96 %, 58,62 % et 8,19 %, respectivement. Bien que la précision de l'estimation de la BA fût faible en raison du port et du mode de croissance des pins des marais, l'emplacement des arbres individuels, la Ht et le V ont été estimés avec une grande précision, en particulier dans des conditions de faible couverture de la canopée. Les efforts futurs basés sur ces résultats pourraient aider à améliorer la précision de l'estimation des attributs à l'échelle de l'arbre comme la BA.

INTRODUCTION

Longleaf pine (*Pinus palustris* Mill.) was once one of the most ecologically important tree species in the southern United States (Oswalt et al. 2012). Historically, longleaf pine forests

Received 16 October 2015. Accepted 13 March 2016.
*Corresponding author e-mail: csilva@uidaho.edu.

spanned an estimated area of 92 million acres (Frost 2006) and were among the most extensive ecosystems in North America (Landers et al. 1995). Today, only 4% of these longleaf pine forests remain (Franklin 2008).

Fire is one of the dominant forces that shape the longleaf pine landscape (Dobbs 2011). Longleaf pine is dependent on fire for successful regeneration and for suppressing hardwood growth (Loudermilk et al. 2011). However, due to fire suppression, much of the remaining longleaf pine forest is in poor or degraded condition. As a result, there has been tremendous interest in longleaf pine conservation, management, and restoration (Brockway 2005).

Successful management of these forests can have sustainable results, because longleaf pines can produce quality wood products when grown in a variety of densities (Franklin 2008). Accurate measures of forest attributes such as tree density (tree/ha), and attributes such as height (Ht), basal area (BA), and stem volume (V) that are used at the tree, plot and stand levels, are essential to management and conservation practices in longleaf pine forests. The most accurate method of estimating these attributes is to physically sample them in the field. However, individual tree field measurements over large areas are limited by budgets and time, making them impractical.

Airborne Light Detection and Ranging (LiDAR) systems have become the dominant remote sensing technique for plot- and stand-level forest inventory, mainly because this technology can quickly provide highly accurate and spatially detailed information about forest attributes across entire forested landscapes (Silva et al. 2014). Increased interest, dataset availability, and technological improvements have greatly expanded the use of LiDAR technologies in forestry over the past decade (Saremi et al. 2014; Hudak et al. 2014; Hansen et al. 2015).

The use of airborne LiDAR to retrieve forest attributes at the tree level is promising, however, not as widely studied as plot- or stand-level approaches. In a tree-level-based modeling approach, individual-tree attributes are usually predicted through 3 steps: (*i*) individual tree detection and metrics extraction, (*ii*) LiDAR- and field-based tree matching, and (*iii*) modeling and prediction. The accurate prediction of tree-level attributes is highly dependent on the methods used to detect and extract individual-tree metrics and forest structure as well (Kankare et al. 2015).

A LiDAR-derived Canopy Height Model (CHM) can be used for detecting individual trees, delineating tree crowns, and subsequently estimating biophysical attributes such as biomass and stem volume (Popescu et al. 2003; Popescu, 2007; Falkowski et al. 2008; Falkowski et al. 2009; Vauhkonen et al. 2012; Hu et al. 2014; Duncanson et al. 2014; Duncanson et al. 2015; Kankare et al. 2015). There are a variety of approaches used to detect and delineate individual trees from LiDAR-derived CHMs. These include identifying local maxima (Popescu et al. 2003; Weinacker et al. 2004; Falkowski et al. 2008; Falkowski et al. 2009) for tree detection, as well as region growth (Hyyppä et al. 2001; Solberg et al. 2006; Pang et al. 2008),valley following (Leckie et al. 2003), and watershed (Chen et al. 2006; Jing et al. 2012) for delineation.

In addition to the individual-tree detection method and forest structure, the accurate prediction of forest attributes at the tree level is also highly dependent on the modeling technique applied (Vauhkonen et al. 2010). Examples of the existing methods for modeling forest attributes at the tree-level from LiDAR data are both parametric (Chen et al. 2007) and nonparametric (Breidenbach et al. 2010; Vauhkonen et al. 2010; Vauhkonen et al. 2012). Saarinen et al. (2014), Vastaranta et al. (2014) and Kankare et al. (2015) have recently tested *k*-nearest neighbor (*k*-NN) imputation for forest inventory modeling at the tree level. In most cases however, *k*-NN imputation, as a nonparametric method, has commonly been used to predict forest inventory attributes at the plot or stand levels (Falkowski et al. 2010; Hudak et al. 2014; Racine et al. 2014). For example, Hudak et al. (2008) evaluated 9 *k*-NN imputation methods and LiDAR data for imputing plot-level BA and tree density (TD) of 11 conifer species occurring in mixed-conifer forests of north central Idaho, USA. Racine et al. (2014) used LiDAR data and *k*-NN imputation to estimate plot age across a managed boreal forest in Quebec, Canada, and Fekety et al. (2015) used repeated field and LiDAR survey data to assess the feasibility of predicting forest inventory attributes across space and time in a conifer forest in northern Idaho, USA.

The aforementioned studies integrated LiDAR and field data in an area-based *k*-NN imputation to predict forest attributes at the plot or stand levels. However, accurate characterization of the forest at the individual-tree level not only enhances conventional and LiDAR area-based forest inventory, but also extends its applications into disciplines where greater detail is valued, such as ecology, wildlife habitat, or biodiversity applications (Goetz et al. 2007; Hinsley et al. 2002; Vierling et al. 2008).

Given that only a fraction of the historic longleaf pine forest ecosystem range remains today, accurate characterization and spatial distribution of individual trees are critical for sustainable forest management and for ecological and environmental protection in longleaf pine forests. Our goal in this study was to predict individual-tree-level attributes using *k*-NN imputation and individual-tree LiDAR-based metrics in a longleaf pine forest in southwestern Georgia, in the United States. Our first aim, therefore, was to evaluate the ability of LiDAR to accurately detect individual trees and determine treetop height (HMAX, m) and crown area (CA, m^2) that are subsequently used for predicting tree attributes. Our second aim was to predict individual tree Ht (m), BA (m^2), and V (m^3) attributes from HMAX and CA metrics using *k*-NN imputation and evaluate its accuracy and precision. This investigation is based on the hypothesis that LiDAR technology and a *k*-NN imputation modeling approach can feasibly provide precise and accurate estimates of these tree attributes in the open canopy structure that is typical of healthy longleaf pine forests.

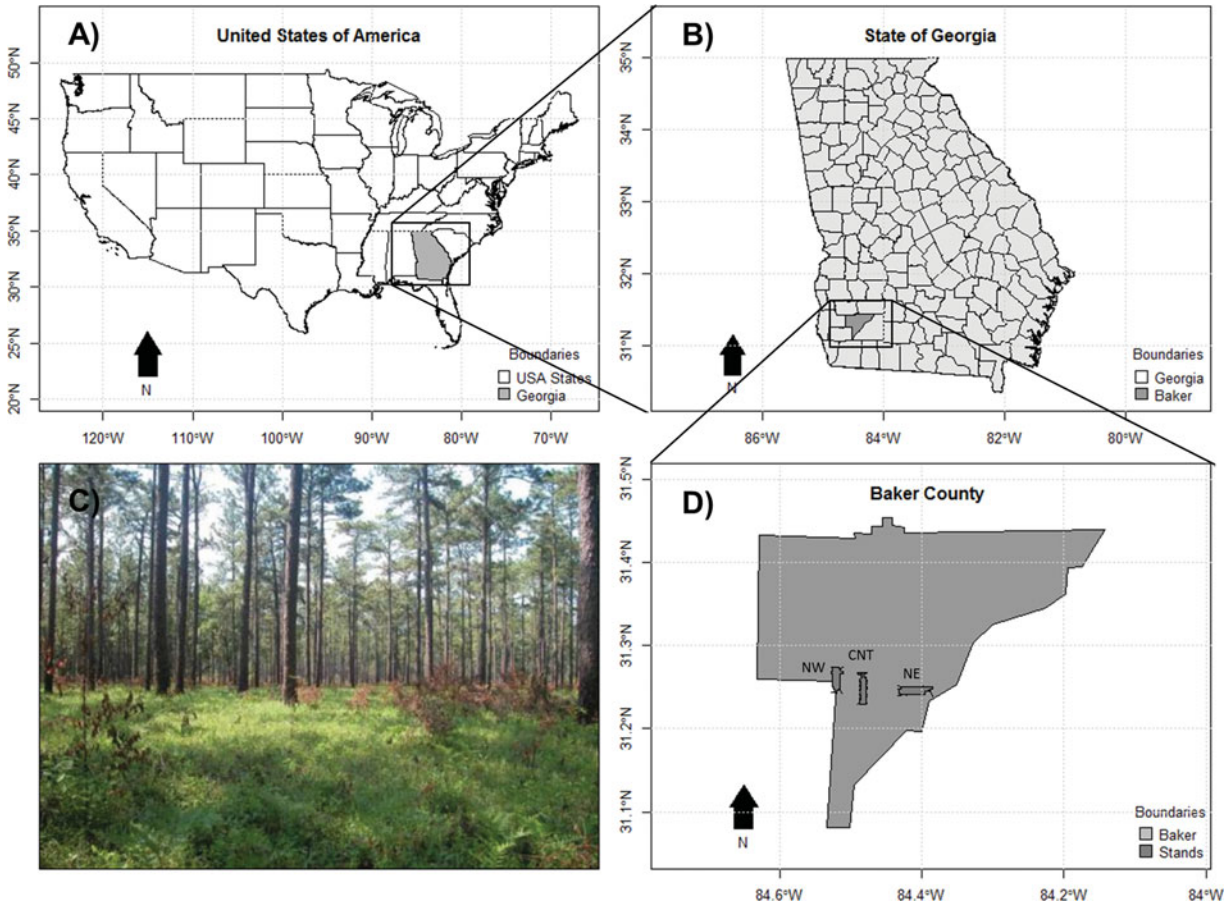

FIG. 1. Longleaf pine forest location: A, B, and D, and profile picture at Ichauway in southwestern Georgia, USA. NW: Northwest; CNT: central and NE: Northeast stands.

MATERIAL AND METHODS

Study Area

The study area for this project is located at Ichauway, an 11,700 ha reserve of the Joseph W. Jones Ecological Research Center in southwestern Georgia, USA (Figure 1). The area is characterized by a humid subtropical climate (Christensen 1981) with a mean annual precipitation of 131 cm fairly evenly spread throughout the year. Mean daily temperatures range from 21 °C to 34 °C in the summer and 5 °C to 17 °C in the winter (Loudermilk et al. 2011). Elevation ranges from 6.23 m to 33.66 m, and the soils are characterized as paleudults, kandiudults, and hapludults with some localized quartzipsamments (Kirkman et al. 2004). The Ichauway reserve has an extensive tract of second-growth longleaf pine managed with low-intensity, dormant-season-prescribed fires at a frequency of about 1–3 years since 1945 (Loudermilk et al. 2011).

In this study, vegetation structure is characterized by an open canopy longleaf pine forest (Figure 1 a, b) and a wiregrass-dominated ground cover maintained under a high-frequency fire regime (Figure 1 c). Maintaining a high-frequency fire regime through repeated application of prescribed fire is a top management goal at Ichauway, with occasional individual-tree selection harvesting for management and research purposes in the natural, second-growth longleaf forests (Palik et al. 2003).

Field Data Collection

The field measurements were carried out from March 2009 to July 2009. A total of 15 rectangular plots (about 4 ha each) were established in 3 stands: CNT, NE, and NW (Figure 1 D). All plots were georeferenced with a geodetic GPS with differential correction capability (Trimble Nomad) with an external Hemisphere Crescent A100 antenna, and all had a horizontal accuracy of < 0.6 m with differential GPS (DGPS) and < 2.5 m without DGPS in open canopy, and 1 m–2 m accuracy with DGPS under forest canopy. All trees were measured for DBH using calipers (two perpendicular measurements at right angles, averaged) or a steel diameter tape, and for Ht using a LaserTech Impulse 200. We also geolocated (UTM E, N) them using the GPS mentioned, and, from these measures, a field-stem map was created. In a few instances, DGPS was not able to resolve locations of multiple small trees in areas with high stocking, and tree locations were recorded by establishing a known DGPS

TABLE 1
Statistical summary of tree measurements attributes at the sample plots

		Tree Density (N/ha)				DBH (cm)				Ht (m)			
Stand	N° Plots	min	max	mean	sd	min	max	mean	Sd	min	max	mean	Sd
NE	7	201	204	202	2	10.00	60.00	30.66	12.11	6.20	31.40	23.01	5.12
CNT	6	126	194	147	25	10.00	74.60	33.21	13.77	6.10	33.30	23.24	4.77
NW	2	77	203	131	61	9.50	71.30	36.29	14.02	8.50	32.10	22.75	4.75

TABLE 2
Statistical summaries of tree basal area (BA) and stem volume (V) at sample plots

	BA (m^2/Tree)				V (m^3/tree)			
Stand	min	max	mean	sd	min	max	mean	sd
NW	0.01	0.40	0.12	0.08	0.04	2.44	0.94	0.47
CNT	0.01	0.44	0.10	0.07	0.01	2.73	1.01	0.50
NE	0.01	0.28	0.09	0.06	0.01	2.28	0.99	0.52

point and then measuring the distance (3 cm–5 cm accuracy) and azimuth (± 0.3 degree accuracy) to those trees with the Impulse 200 and MapStar Compass module, respectively. The mean longleaf pine tree Ht and DBH measured in our study area was 22.95 (±4.88) m and 32.87 (±13.30) cm, respectively, and the number of trees per hectare (N/ha) was approximately 147 (±29) trees. A statistical summary of the tree density, Ht, and DBH field measurements are presented in Table 1.

The outside-bark V was obtained via a longleaf pine allometric equation according to Gonzalez-Benecke et al. (2014) (Equation 1). The equation has a coefficient of determination (R^2) of 0.78 and absolute and relative root mean square error (RMSE) of 0.17 m^3 and 38.21%, respectively.

$$\ln(V) = -9.944543 + 3.123691^{*}\ln(Ht). \quad [1]$$

In addition to V, tree-level BA was also computed. Statistical summaries of the reference BA and V calculations are presented in Table 2.

LiDAR Data and Preprocessing

LiDAR data were acquired using an Optech GEMINI Airborne Laser Terrain Mapper (ALTM) mounted in a twin-engine Cessna Skymaster (Tail Number N337P). The survey was carried out on March 5, 2008. LiDAR flight parameters are presented in Table 3.

LiDAR preprocessing was performed using US Forest Service FUSION/LDV 3.42 software (McGaughey 2015) and LAStools (Isenburg 2015). The workflow is graphically shown in Figure 2a. First, in FUSION/LDV, the quality of the LiDAR dataset was visually evaluated, and a simple report using the Catalog tool was generated. A filtering algorithm based on Kraus and Pfeifer (1998) was applied to differentiate between ground and nonground returns. DTMs were generated using the classified ground points with a spatial resolution of 1.0 m, using the GridSurfaceCreate function. The CanopyModel tool was then used to interpolate vegetation points and to generate DSMs with a spatial resolution of 0.5 m. Afterward, the ClipData tool was applied with the height and dtm switches to normalize heights and to assure that the z coordinate for each point corresponded to the height above ground and not the orthometric elevation of the single point. The PolyClipData tool was then used to make a subset of the LiDAR points within each of the 15 in situ measured test plots. The CloudMetrics tool with a height and cover thresholds of 1.37 m (Nilsson 1996) were used to compute the canopy cover (COV,%), within sample plots. COV was

TABLE 3
LiDAR flight parameters

LiDAR Survey Parameters	
Scan Frequency	45 Hz
Scan Angle	+/− 20 deg
Scan Cutoff	+/− 4.0 deg
Scan Offset	0 deg
System PRF	125 kHz
Swath Width	344.64 m
Flying Altitude	600m AGL
Down Track Resolution	0.75 m
Points per square meter	5.06
Horizontal Datum	NAD83
Vertical Datum	NAVD88 (GEOID 03)
Projection	UTM Zone 16N

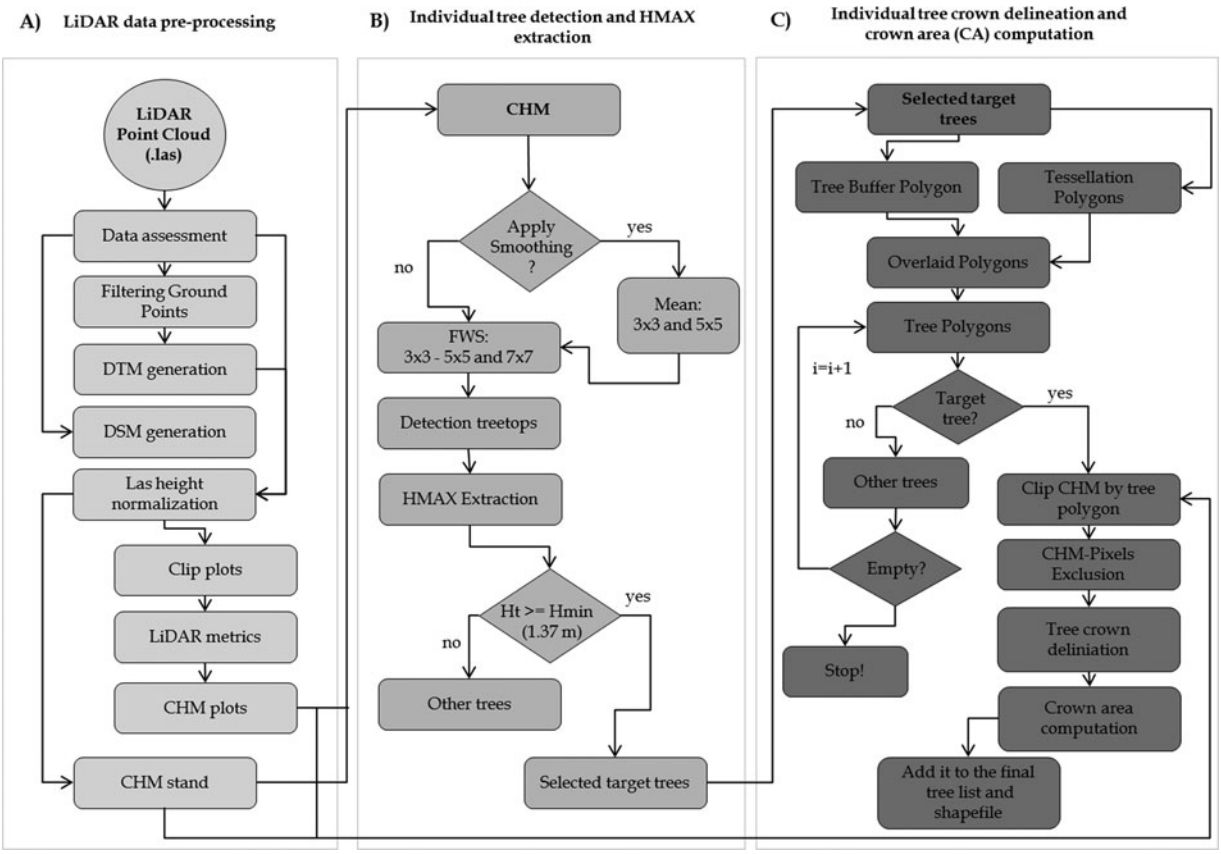

FIG. 2. Flowchart of the LiDAR data processing.

calculated as the number of LiDAR first returns above 1.37 m, divided by the total number of first returns. Such LiDAR-derived CHM often contain height irregularities within individual-tree crowns—so-called data pits—which reduce accuracy in tree detection and subsequent extraction of biophysical parameters (Gaveau and Hill 2003, Shamsoddini et al. 2013). Therefore, the pit-free algorithm, developed by Khosravipour et al. (2014) was used to generate a pit-free CHM at 0.5-m spatial resolution though a workflow implemented in LAStools (Isenburg 2015).

Individual Tree Detection and HMAX Extraction

Individual tree detection was performed in R (R Development Core Team 2015) using the FindTreesCHM function from the rLiDAR package (Silva et al. 2015). The FindTreesCHM function uses a local maximum algorithm to search for treetops in the CHM through a moving window with a fixed treetop window size (TWS; Wulder et al. 2000). To achieve optimal tree detection, we tested 3 TWS (3 × 3, 5 × 5, and 7 × 7) first on an unsmoothed CHM, and then on a CHM smoothed by a mean smooth filter with fixed smoothing window size (SWS) of 3 × 3 and 5 × 5. Even when the smoothed CHM option was used to find trees, the treetop heights (HMAX) were extracted from the unsmoothed CHM.

A total of 15 test subplots (30 m × 30 m) were randomly situated within each of the 15 plots (1 subplot per plot), and the number of trees detected (NTD) per subplot from LiDAR were manually compared with field-based data and evaluated in terms of true positive (TP, correct detection), false negative (FN, omission error) and false positive (FP, commission error). The accuracy of the detection was further evaluated for recall (r), precision (p) and F-score (F) according to Li et al. (2012), using the following equations (Goutte and Gaussier 2005; Sokolova et al. 2006):

$$r = \frac{TP}{TP + FN}. \quad [2]$$

$$p = \frac{TP}{TP + FP}. \quad [3]$$

$$F = 2 * \frac{r * p}{r + p}. \quad [4]$$

Note that recall is inversely related to omission error and represents the tree-detected rate. Precision is inversely related to commission error and describes the rate of correct detections. F-score is used to represent the harmonic mean

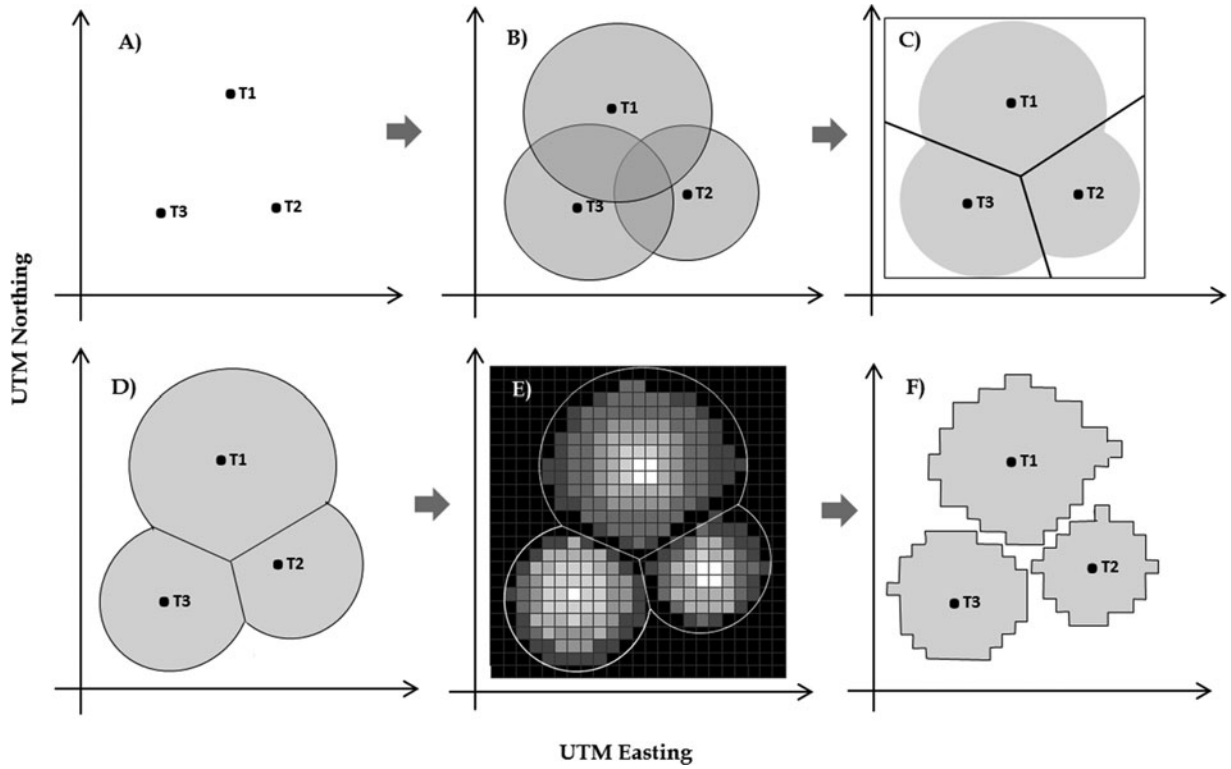

FIG. 3. Illustration of the individual tree crown delineation algorithm. T = trees. (A) treetops; (B) buffer search area of 10 m maximum radius; (C) Centroidal Voronoi Tessellation delineation; (D) buffer and Centroidal Voronoi Tessellation overlaid area; (E) CHM clipping; (F) crown delineation.

of recall and precision, which takes both commission and omission errors into consideration. Hence, a higher F-score indicates that both commission and omission errors are lower (Li et al. 2012). Recall, precision, and F-score ranges from 0 to 1, and the F-score will become higher with higher p and r values.

Individual Tree Crown Delineation and Crown Area Computation

Tree-crown delineation was also performed in R, using the ForestCAS function from the rLiDAR package (Silva et al. 2015). Inputs to this process were the smoothed CHM in addition to the tree-location output described in the previous steps. The algorithm implemented in the ForestCAS function is shown in Figure 2c and Figure 3, and follows the example presented in the figure illustrating 5 hypothetical trees (Figure 3a). The algorithm starts by applying a variable radius crown buffer (Figure 3b) to delimit the initial tree crown area. In this study, the variable radius was calculated for each tree by multiplying the LiDAR-derived tree height by 0.6, because preliminary field observation revealed that the tree crown radius typically was not larger than 60% of the LiDAR-derived tree height. After determining the merged tree polygon using the first area delimitation (Figure 3b), we then split the data using the centroidal voronoi tessellation approach (Aurenhammer and Klein 1999) to isolate each individual-tree polygon (Figure 3c,d). After isolating each tree polygon, we clipped them from the CHM and excluded the grid cells with values below 30% of the HMAX in each specific detected tree (Figure 3e) to eliminate the low-lying noise. Finally, the tree-crown delineation and crown area (CA, m^2) were computed by delimiting the boundary of grid cells belonging to each tree (Figure 3f).

rSTree: Searching for the LiDAR and Reference Trees

Forest inventory and modeling of individual trees using field and LiDAR data is a highly desirable approach. However, to develop this type of modeling approach, the challenge is to match LiDAR-delimited trees with reference trees measured in the field. In many cases, the tree-location reference measured in the field is inaccurate (often due to GPS error), complicating the individual-tree-level modeling approach. Instead of manually moving reference tree locations to match with the tree locations detected from LiDAR, we developed a novel approach for matching LiDAR and field trees automatically (Figure 4). The proposed rSTree algorithm uses the acceptable maximum Euclidian distance (MED) and minimum height difference (MHD) computed between LiDAR and field-based data, in terms of tree location and height, respectively, as the imputed parame-

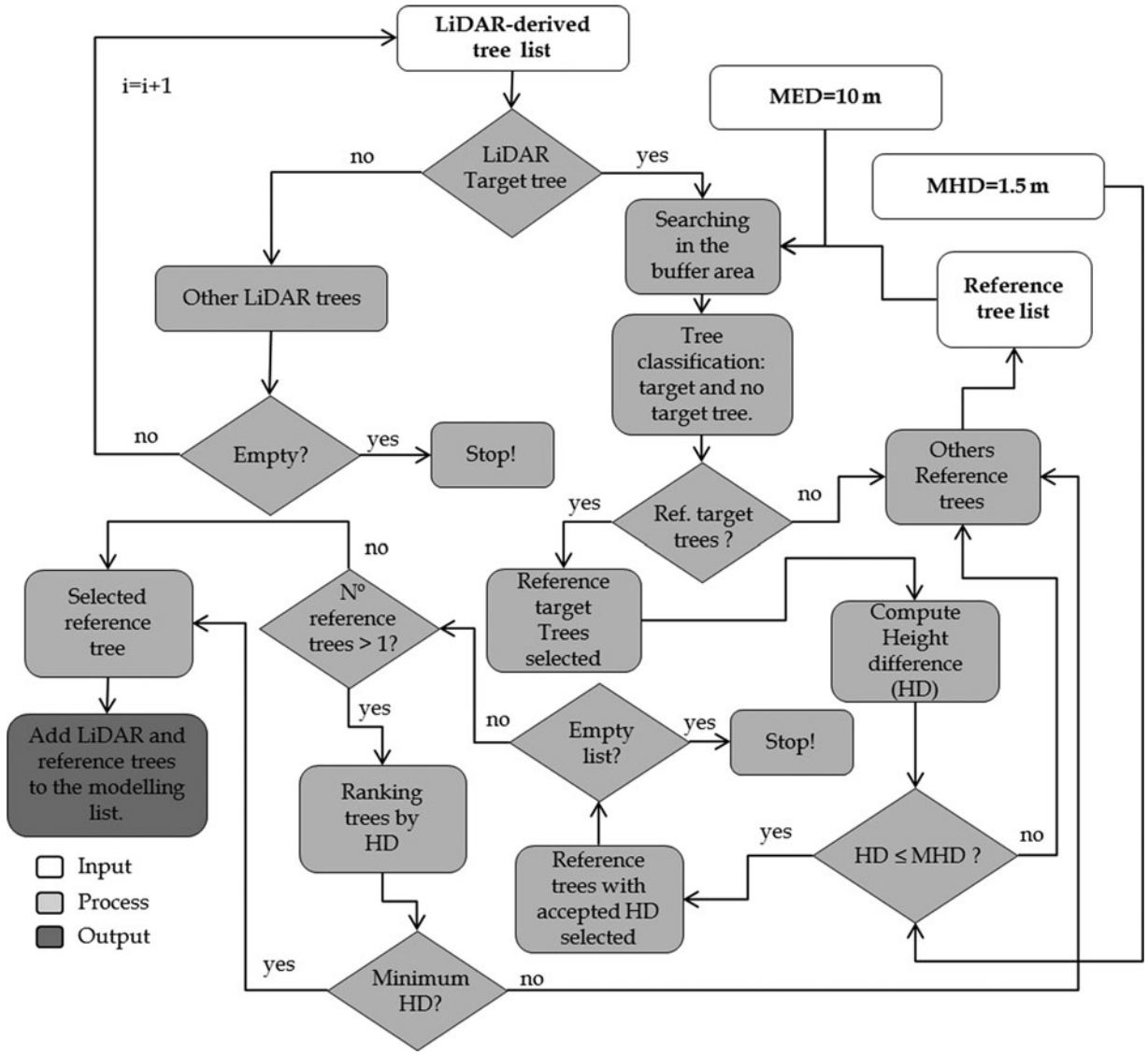

FIG. 4. rSTree algorithm: searching for the LiDAR and reference trees. MED = maximum Euclidian distance, MHD = minimum height deference, HD = height difference.

ters. The algorithm processes a single match tree at a time, and it starts with the first detected LiDAR tree. The user-defined MED parameter is then used to buffer a search area for a possible matching tree. In this study, we used 10 m, because, given the GPS errors, we are assuming that the reference tree is within a radius of 10 m. The field-based trees located inside the search area are selected. Trees with height difference (HD) $\leq$ MHD are then selected for the next step as target trees. In this study, we used MHD = 1.5 m, because most of the literature for conifer LiDAR versus field stems have reported a RMSE in height of $\sim$1 m–2 m (e.g., Vastaranta et al. 2015). In an open canopy forest such as longleaf pine presented herein, we are assuming that the error in LiDAR height would not exceed 1.5 m. If more than one reference field-based tree has HD $\leq$ MHD, the trees are ranked by HD and the tree with the smallest HD is selected. If 2 or more field-based trees have a perfect match in terms of smallest HD and distance to the detected tree, we randomly selected one as the target field-based tree to match with the LiDAR tree. After all interactions, the LiDAR and reference trees are combined, added, and exported as a table for the individual-tree-level attributes modeling approach.

Imputation Modeling Development

In this study, because the height–diameter allometry for longleaf pine breaks down after reaching a diameter of $\sim$25 cm, when height growth asymptotes at $\sim$25 m (Gonzalez-Benecke et al. 2014), we believed that a nonparametric modeling tech-

nique to predict forest attributes at tree level would be more appropriate than a parametric model. Therefore, *k*-NN imputation, a nonparametric technique, was conducted using the yaImpute (Crookston and Finley 2008) package in the R statistical software (R Core Team 2015). Many imputation methods can be used for associating target and reference observations, however, recent studies have shown that the Random Forest (Breiman 2001) approach generally produces better results compared to other imputation methods (Hudak et al. 2008; Nelson et al. 2011;Waske et al. 2012). For this study, we used Random Forest-based *k*-NN (RF *k*-NN) to characterize the relationships between predictor (HMAX and CA) and response (Ht, BA, and V) variables used for imputation. The number of neighbors was set to one ($k = 1$) to maintain the original variance in the data (Hudak et al. 2008). The dataset for the modeling process was randomly split into subsets with 75% for training and 25% for testing, and a total of 1,000 regression trees were fitted in the RF *k*-NN model.

Model Assessment

Accuracy of the imputation model was assessed by calculating the absolute and relative root mean square distance (RMSD, RMSD%) and bias (BIAS, BIAS%) between imputations and observations (Stage and Crookston 2007), computed for a single response variable as follows:

$$\mathrm{RMSD} = \sqrt{\frac{\sum_{i=1}^{n} (I_i - O_i)^2}{n}}, \quad [5]$$

$$\mathrm{BIAS} = \frac{1}{n} \sum_{i=1}^{n} (I_i - O_i) \quad [6]$$

where I is the imputed value of a variable, O is the observed value, and n is the number of reference observations. The RMSD is analogous to the RMSE used to assess regression model accuracy (Stage and Crookston 2007). The relative RMSD and BIAS are computed by dividing absolute RMSD and BIAS by the mean of the variable computed over the reference observations and multiplied by 100. We defined acceptable model precision and accuracy as a relative RMSD and Bias of $\leq$15% to have a model precision and accuracy less than or equal to the conventional forest inventory standard in the longleaf pine.

We also employed statistical equivalence tests to assess whether the imputed tree attributes are statistically similar (i.e., equivalent) to the field-based attributes (Robinson et al. 2005). According to Smith et al. (2009), statistical equivalence tests are used to test the null hypothesis of "no substantial difference" between 2 sample populations (H0: the sample populations are different; H1: the sample populations are equivalent). We employed a regression-based equivalence test to test for intercept equality (i.e., the mean of imputed tree attribute is equal to the mean of the field-based attribute) and slope equality to 1 (i.e., if the pairwise, imputed and observed, attributes are equal, the regression will have a slope of 1). A description of equivalence tests can be also found in the "equivalence" package in R (Robinson, 2015), and examples of equivalence plots in LiDAR studies can be found in Falkowski et al. (2008), Smith et al. (2009), Hudak et al. (2012), and Silva et al. (2014).

Stand-Level Imputation of Tree Attributes

According to Falkowski et al. (2008), tree-detection accuracy decreases with increasing COV. An adaptive approach using COV as a constraint to select the best parameters of TWS and SWS for tree detection was developed in this study. Therefore, we tiled the normalized point cloud using a grid-layer of 200 m $\times$ 200 m square plots, and for each single tile we computed COV, which was calculated by the number of LiDAR first returns above 1.37 m, divided by the total number of first returns. A buffer of 30 m was applied over each single square layer to remove the edge effect of the individual tree detection. As the parameters of the tree detection at stand level was dependent on the results from the test plots, our hypothesis was that small TWS would provide better results in close canopy area, and vice versa. In the buffer overlaid areas, after tree detection using the FindTreesCHM function from the rLiDAR package (Silva et al. 2015), 1 of 2 trees detected was automatically removed to avoid overdetection. Afterward, tree-crown delineation was performed across the entire stand, using the ForestCAS function from the rLiDAR package (Silva et. al 2015). The RF *k*-NN imputed model based in the test plots was then applied, and the tree attributes Ht, BA, and V were estimated for each single tree across all stands.

RESULTS

Stand-Level Characterization from Field Data and Lidar-Based Plot Metrics

According to the LiDAR-derived HMAX value, canopy height of the longleaf pine forest was similar across the 3 stands (Figure 5a). LiDAR-derived COV indicated a decrease in percent canopy cover from the NW to CNT and NE stands, whereas COV variance increased (Figure 5b). Although the stands are similar in height, they are different in terms of field-measured tree density. As observed in the description of the sites in the material and methods section, the NW stand had highest tree density and the NE stand had the lowest, whereas the variance in tree density showed the opposite trend in COV (Figure 5c).

Individual-Tree Detection

The individual-tree detection results from the test plots are shown in Table 4. The TWS and SWS combination were sensitive parameters in terms of tree detection. The TWSs that provide better results were 5 $\times$ 5 and 7 $\times$ 7, with a tree detection overall improvement of 58.25% and 34.59% compared to

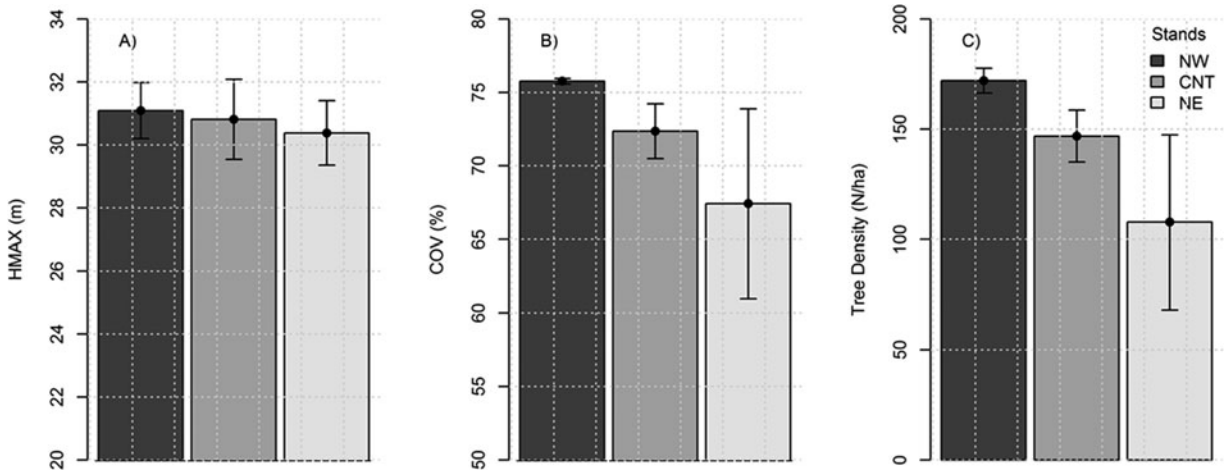

FIG. 5. LiDAR-based plot (A) HMAX and (B) COV; and (C) tree density measured in the field at the longleaf pine test plots. Error bars indicate standard deviations.

the 3 × 3, respectively. The relationship between SWS and the NTD from LiDAR was inversely proportional. Smaller TWSs, such as 3 × 3, detected more trees compared to large TWSs, such as 7 × 7, causing an overestimation of NTD. In general, TWS of 3 × 3 for the CHM smoothing provided better results.

Although different combinations of TWS and SWS parameters might provide a better performance in each test plot, we identified a positive and strong nonlinear relationship between the number of reference trees and LiDAR-derived COV (Figure 6a). Therefore, in an effort to be consistent and replicable, we decided to use the adaptive approach already cited in the

TABLE 4
Individual tree detection in the test subplots

				TWS								
				3 × 3			5 × 5			7 × 7		
				SWS			SWS			SWS		
Ref. (N)	Stand	COV	Ref. (N)	NF	3 × 3	5 × 5	NF	3 × 3	5 × 5	NF	3 × 3	5 × 5
1	NW	68.39	803	4675	1112	587	1246	702	478	620	507	413
2		75.63	815	4725	1156	586	1312	674	480	639	514	410
3	CNT	70.40	519	4063	893	467	1028	515	393	485	399	340
4		70.96	503	4346	939	490	1079	548	410	526	425	370
5		71.47	572	4256	1021	536	1131	632	437	570	467	381
6		72.62	543	4208	953	505	1096	584	426	550	440	385
7		73.17	777	4222	1052	577	1110	622	449	552	452	383
8		75.53	621	4723	1050	573	1221	620	465	609	483	410
9	NE	60.13	321	2994	684	346	750	373	272	344	275	243
10		61.75	306	3222	701	363	771	414	283	374	300	250
11		63.85	366	3366	750	393	852	427	319	414	323	292
12		63.96	338	3319	743	370	849	396	292	411	318	265
13		72.24	737	4006	940	510	1018	563	405	521	436	368
14		74.50	810	4379	1012	547	1119	612	437	530	463	385
15		75.56	797	4357	1023	561	1145	620	452	567	454	391

The highlighted gray color represents the best results, which were determined by comparing the number of trees detected (NTD) to the field-based tree inventory number (N). The closest values of NTD compared with N were selected as the best results.

Ref.: reference number of tree per test plot (N); TWS: fixed treetop windows size; SWS: fixed smoothing windows size; NF: no filter applied; NE: Northeast stand; CNT: Central stand and NW: Northwest stand.

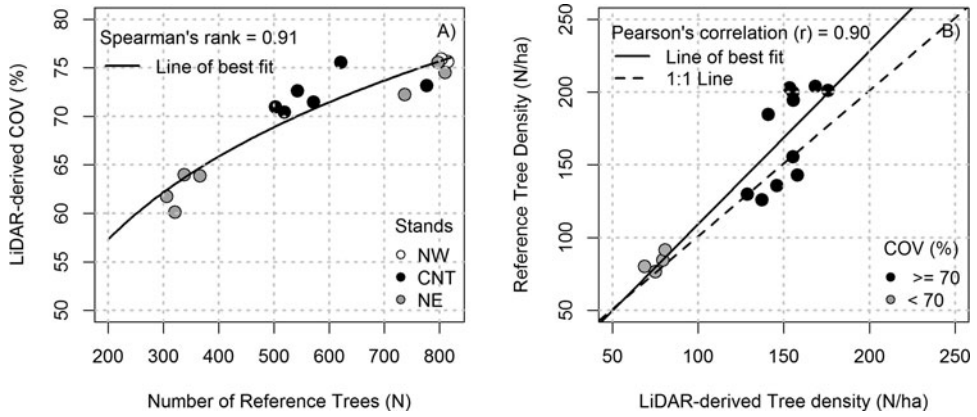

FIG. 6. LiDAR-derived COV versus number of reference trees (N) measured in the field (A), and LiDAR-derived versus reference tree densities.

methods section, in which the COV is used as an auxiliary variable to select the TWS in each test plot. For the sample plots with COV $> = 70\%$, the 5×5 TWS was selected and in plots with COV $< 70\%$ the 7×7 TWS was selected. Additionally, the 3×3 SWS was selected to be applied across all test plots, because it in general provides more accurate results (Table 4).

The relationship between the reference and LiDAR-derived number of trees per test plot according to the adaptive approach mentioned is shown in Figure 6b. Our method slightly underestimates the number of trees, especially in the test plots with COV $> 70\%$. However, the correlation between reference and NTD per hectare (N/ha) is relatively strong, displaying a correlation coefficient of 0.90.

The accuracy assessment results for individual-tree detection in the 15 test subplots is shown in Table 5. The recall varies from 0.74 to 1, with the overall value of 0.82; the value of p varies from 0.71 to 1, with the overall value of 0.85; and the F-score, which considers both of these last 2 factors, varies from 0.74 to 1, with the overall value from all the plots of 0.83. There are 185 reference trees in our test subplots, and only 177 (81.6%) trees were detected. In summary, the algorithm missed 34 (14.1%) trees, and falsely detected 26 (18.1%) trees, with underdetection outweighing overdetection (Table 5 and 6).

TABLE 5
Accuracy assessment results of LiDAR-based individual tree detection according to recall (r), precision (p) and F-score (F) statistics parameters

		Number of Trees Detected (NTD)							
Subplots	COV (%)	LiDAR	Reference	FP	FN	TP	r	p	F
1	46.21	13	16	1	4	12	0.75	0.92	0.83
2	46.87	16	18	2	4	14	0.78	0.88	0.82
3	50.66	8	6	2	0	6	1.00	0.75	0.86
4	56.55	5	5	0	0	5	1.00	1.00	1.00
5	60.31	4	4	0	0	4	1.00	1.00	1.00
6	63.02	4	4	0	0	4	1.00	1.00	1.00
7	64.71	9	8	1	0	8	1.00	0.89	0.94
8	67.13	7	5	2	0	5	1.00	0.71	0.83
9	71.41	16	17	3	4	13	0.76	0.81	0.79
10	71.45	18	21	2	5	16	0.76	0.89	0.82
11	74.33	20	23	4	7	16	0.70	0.80	0.74
12	76.93	11	10	2	1	9	0.90	0.82	0.86
13	80.56	23	27	3	7	20	0.74	0.87	0.80
14	85.58	15	13	3	1	12	0.92	0.80	0.86
15	83.48	8	8	1	1	7	0.88	0.88	0.88
Overall	66.41	177	185	26	34	151	0.82	0.85	0.83

TABLE 6
Accuracy assessment results for the individual-tree detection as a function of LiDAR-derived COV

	Number of Trees Detected (NTD)							
COV (%)	LiDAR	Reference	FP	FN	TP	r	p	F
≤ 70	60	53	9(17.0)	2(3.8)	51(96.2)	0.96	0.85	0.90
>70	117	132	17(12.9)	32(24.2)	100(75.8)	0.76	0.85	0.80
Overall	177	185	26(14.1)	34(18.1)	151(81.6)	0.82	0.85	0.83

FP: False positive; FN: False negative; TP: True positive; r: recall; p: precision and F: F-score.

The strongest results were obtained in test subplots with COV < 70%, with 96% of the trees detected, commission and omission errors limited to 17.0 and 2% and an F-score of 0.90. When considering test subplots with COV > 70%, the algorithm detected 76% of trees with commission and omission errors of 13% and 24%, respectively (Table 6). The relationship between the F-score and COV is shown in Figure 7. The correlation is relatively strong, with a correlation coefficient of 0.91.

The LiDAR-derived HMAX ranged from 5.24 m to 31.91 m with mean and standard deviation (SD) of 24.39 m and 3.18 m, respectively. The LiDAR-derived CA ranged from 3.0 m^2 to 204.5 m^2, with mean and SD of 50.2 m^2 and 24.74 m^2, respectively. The distributions of HMAX and CA are shown in the Figure 8.

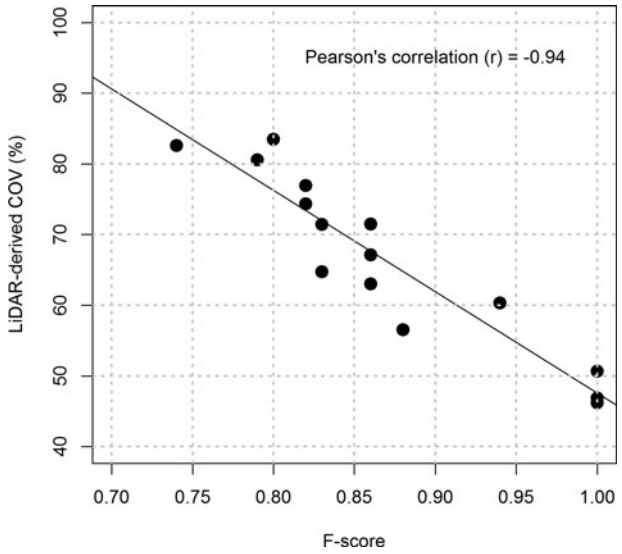

FIG. 7. Relationship between LiDAR-derived COV and F-score in the 15 test subplots.

Imputation Modeling Estimates at Tree Level at the Test Plots

The rStree algorithm matched 4,242 detected trees to field-based trees (48.0%). From this total, 3181 (75%) trees were used as training and 1061 (25%) trees were used as testing data for imputation modeling.

The HMAX and CA metrics were better predictors of Ht and V than BA. The imputed training model produced a relative RMSD of 2.56%, 57.33% and 7.49%; relative BIAS of 0.08%, −0.50% and 0.22%, and pseudo-R^2 of 0.96, 0.22, and 0.95 for the Ht, BA, and V attributes, respectively.

The imputed and observed Ht and V attributes from the validation dataset were statistically equivalent at the 25% rejection region (Figure 9a,c). However, the imputed and observed BA

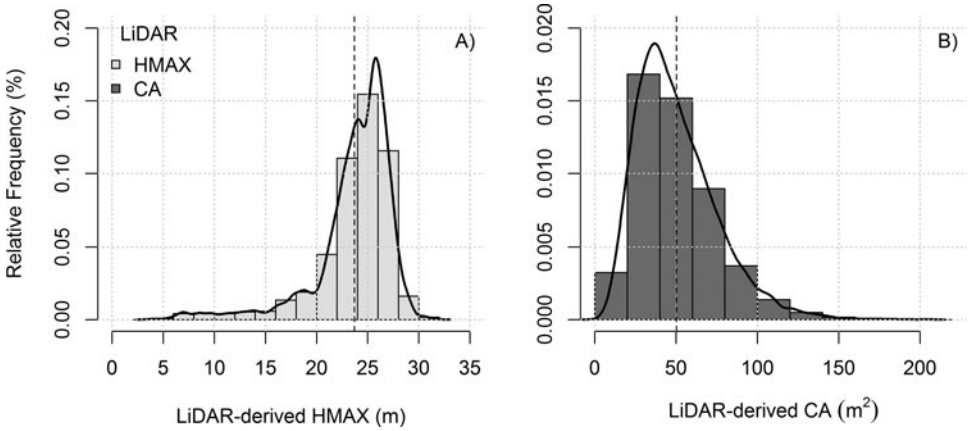

FIG. 8. Distribution of LiDAR-derived (A) HMAX and (B) CA values. The black line representsd a fitted distribution.

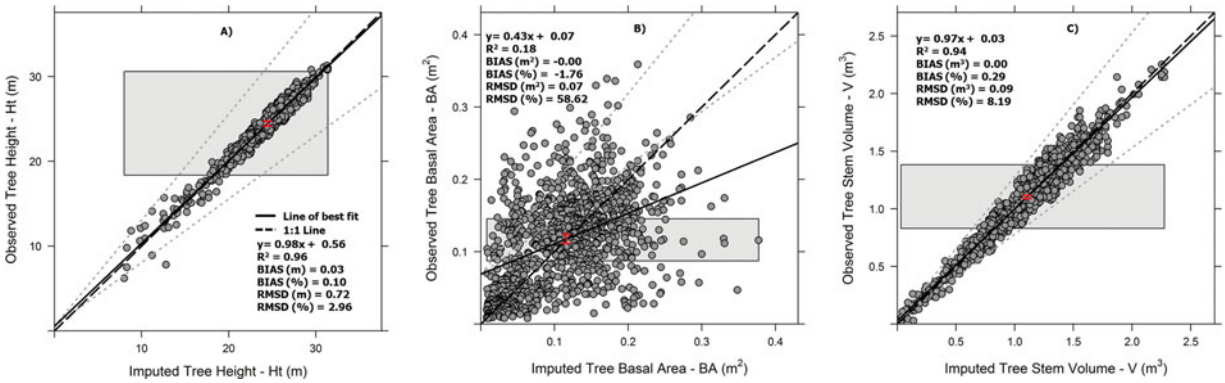

FIG. 9. Equivalence test graphs for the imputed and observed longleaf pine tree attributes. (A) Tree Height Ht (m); (B) Tree Basal Area - BA (m2); (C) Tree Stem Volume - V (m3), N = 1061. The equivalence plots design presented herein are an adaptation of the original equivalence plots presented by Robinson (2015). The grey polygon represents the ± 25% region of equivalence for the intercept, and the red vertical bar represents a 95% confidence interval for the intercept. The imputed tree attributes are equivalent to the reference attributes when the red bar is completely within the grey polygon. If the grey polygon is lower than the red vertical bar, the imputed attributes are biased low; if it is higher than the red vertical bar, the imputed forest attributes are biased high. The grey dashed line represents the ± 25% region of equivalence for the slope, and the red vertical bar is contained completely within the grey dashed line, the pairwise measurements are equal. A bar that is wider than the region outlined by the grey dashed lines indicates highly variable predictions. The gray dots are the pairwise measurements, and the solid line is a best-fit linear model for the pairwise measurements. The black dashed line represents the 1:1 line.

values were not statistically equivalent at the 25% rejection region (Figure 9b). The Ht and V imputation models produced estimates that were strongly ($r > 0.97$) correlated with the validation inventory dataset, whereas the BA imputation model produced estimates of BA that were weakly correlated ($r = 0.42$) with the validation data. The RMSD and BIAS values were relatively low, whereas pseudo-R^2 values were high for the Ht and V. On the contrary, the RMSD and BIAS was relatively high, and the pseudo-R^2 relatively low, for the BA estimates. The distributions of imputed and observed forest attributes across all stands from the testing dataset are shown in the Figure 10. In general, the similarity between the observed and imputed attributes is high.

Stand-Level Forest Attributes Estimates

The N of trees detected in the stands ranged from 35,980 to 52,184; mean tree Ht ranged from 21.10 to 23.17 m; mean tree BA ranged from 0.09 to 0.10 m^2 and mean tree V ranged from 0.79 to 0.96 m^3, as presented in Table 7 Mean stand-level BA was 10.73 m^2/ha (SD = 2.69 m^2/ha) and mean stand-level V was 99.94 m^3/ha (SD = 26.25 m^3/ha). We also graphed histograms of imputed values for each stand and the shape of these distributions (Figure 11). The distributions show that the NW stand is the most mature, the NE stand has the highest proportion of smaller trees, and the CNT stand has an intermediate structure. These distributions provide more information that is subsumed within the Ht, BA, and V mean and standard deviation trends between stands, as summarized in Figure 5.

DISCUSSION

Individual Tree Detection

Accurate individual-tree attributes are critical for forest assessment and planning. This study presents a simplified framework for automated, LiDAR-based individual-tree detection and modeling procedure for estimating tree attributes. The results presented herein demonstrate that the total number of trees can be derived with satisfactory accuracy.

We found that the successful identification of tree locations using the local maximum technique depends on the careful selection of the TWS. If the TWS is too small or too large, errors of commission or, respectively, omission occur, as was also reported by Wulder et al. (2000). Tree-detection accuracy was greatly affected by the different TWS and SWS combinations tested (Table 4). TWS was inversely proportional to the number of trees detected in general. Because COV is directly proportional to tree density in general, larger TWS is generally more appropriate in open canopy forest structures. In this study, 70% COV was the threshold chosen as the TWS; this is substantially higher than the 50% threshold reported in previous studies (Falkowski et al. 2008) and represents a significant advance in our ability to extract individual-tree attributes from denser coniferous forest canopies. Even though different combination of TWS and SWS would provide high accuracies in certain local areas, a consistent TWS parameter is also advantageous for automated tree detection across large spatial extents, and therefore, we employed the COV variable as a criterion for adapting the TWS.

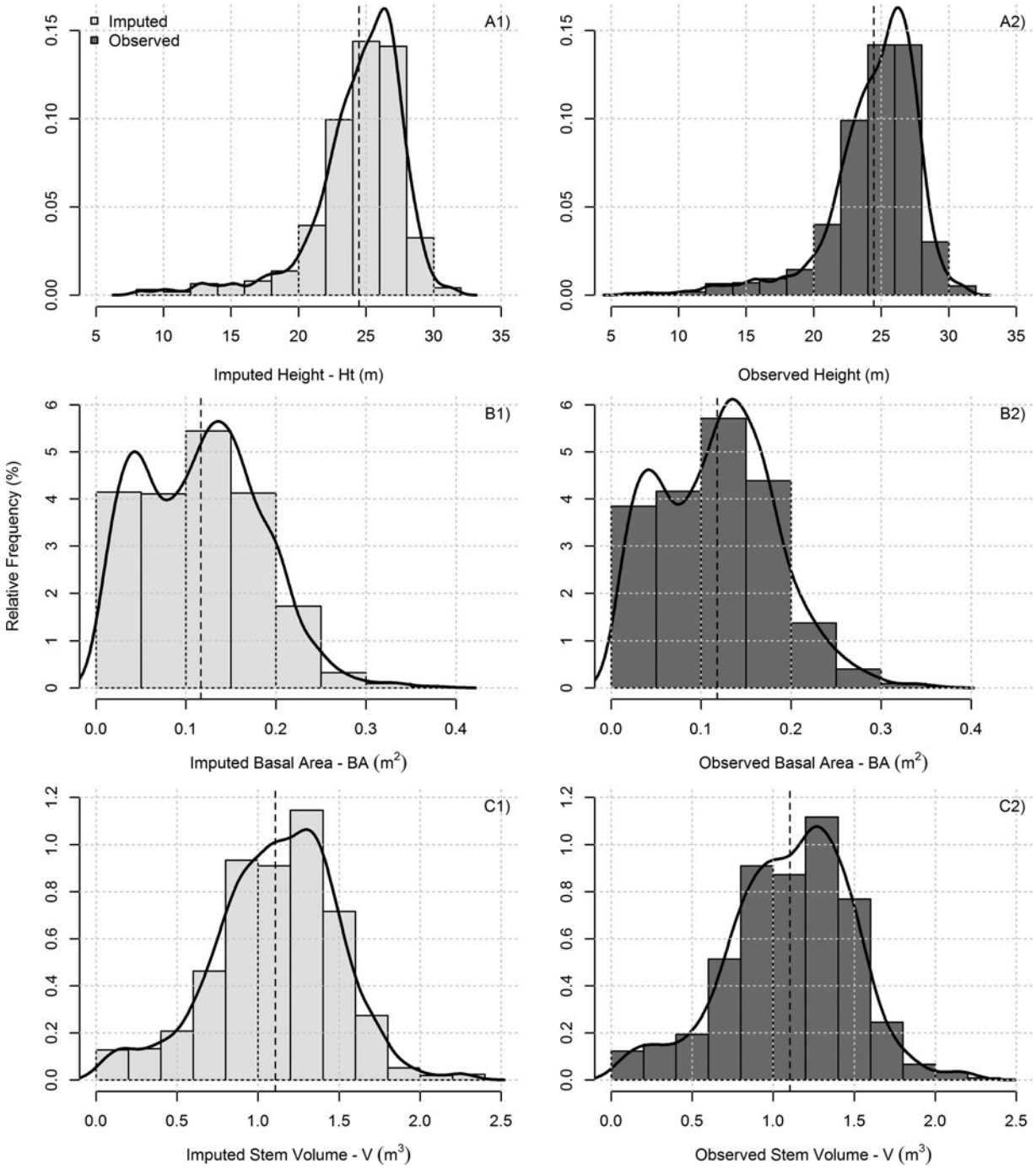

FIG. 10. Imputed and observed tree attributes distribution from the testing dataset. (A), (B) and (C) represent Ht, BA, and V distribution across the 3 stands. The numbers 1 and 2 represent the imputed and observed values. The black line represents a fitted distribution, and the dashed vertical line represents the mean.

Smoothing is a common technique applied to LiDAR-derived CHMs for individual tree detection purposes. In this study, we tested the mean smoothing filter as a smoother. Khosravipour et al. (2014) reported that the performance of individual-tree detection was better using pit-free CHMs instead of a standard smoothed Gaussian CHM (in a coniferous plantation forest in Barcelonnette basin, southern French Alps, France). We observed the same improvement, but then further applied the 3 × 3 SWS over the pit-free CHM to produce even more accurate results. Applying the 3 × 3 SWS the irregular crown shapes that

TABLE 7
Estimated tree attributes summarized at the stand level

		Ht (m)		BA (m^2)			V (m^3)		
Stands	NTD	Mean	Sd	Mean	Sd	Total	Mean	Sd	Total
NW	36958	23.17	4.14	0.10	0.07	3824.11	0.96	0.40	35658.33
CNT	52184	21.26	5.34	0.09	0.07	4478.04	0.80	0.49	42114.29
NE	35980	21.10	5.42	0.09	0.07	3119.95	0.79	0.49	28564.40

NTD = Number of Trees Detected

typify longleaf pine tree crowns (compared to other conifers, which tend to have a more regular, conical shape), thus eliminating spurious local maxima caused, for example, by longleaf pine tree branches that were not already removed by the pit-free CHM itself. Filter sizes and the conditions for filtering the CHM must be carefully tested and selected for different forest types (Lindberg and Hollaus 2012).

The tree-detection results from this study are comparable to the results obtained in other studies using both point cloud and raster-based approaches. Li et al. (2012), using a new method for segmenting individual trees from the LiDAR point cloud in a mixed conifer forest on the western slope of central Sierra Nevada Mountains of California, USA, showed that the algorithm detected 86% of the trees ("recall"), and 94% of the trees were segmented correctly ("precision"), with an overall F-score of 0.90. Vega et al. (2014), using the PTrees algorithm to segment individual trees in a conifer plantation in southwestern France, reported overall recall, precision, and F-score of 0.93%, 0.98%, and 0.95, respectively. Khosravipour et al. (2014), comparing the accuracy of individual-tree detection from the LiDAR-derived Gaussian smoothed and pit-free CHMs in mixed forest in southern French Alps in France, achieved an overall accuracy of 70.6% and 74.2%, respectively, from high-density LiDAR, and 35.7% and 67.7%, respectively, from artificially thinned, low-density LiDAR data. Lähivaara et al. (2014), using a Bayesian approach to tree detection based on LiDAR data, reported an accuracy of 70.2% for 2751 trees measured across 36 different field plots in a managed boreal forest in Eastern Finland. Maltamo et al. (2004), in state-owned forest located in Kalkkinen, southern Finland, using local maximum and segmentation techniques, detected only 39.5% of all trees, although the proportion of detected dominant trees was as high as 83.0%.

In this study, the accuracy of individual-tree detection measured by the F-score, as expected, was inversely proportional to forest COV. Overall, commission errors were more prevalent in less dense test plots, and omission errors were more common where crowns overlapped. Previous research has shown that tree-detection accuracy decreases with increasing canopy cover (Falkowski et al. 2008). As also reported in Falkowski et al. (2008), the influence of GPS error is also an unquantifiable source of uncertainty in the current study. Popescu (2007) reported that treetop positions might be determined with higher accuracy using a CHM image rather than error-prone measurements derived from differential GPS in the field. Even though we collected at least 20 GPS positions at each tree and performed a differential correction, it can be argued that the field GPS tree location is less accurate than the treetop location detected from LiDAR, especially in high-canopy-cover conditions that can degrade field GPS accuracy (Wing et al. 2008). For example, in Figure 12, the reference tree location represented by the black point (Figure 12a) and vertical black line (Figure 12b,c) are located far away from the treetop location (white point, Figure 12a) and the point cloud peaks (Figure 12b). This leads to a less accurate stem map in areas with high COV, ultimately making it very difficult to objectively determine if a sample tree had actually been detected in high-canopy-cover situations. Moreover, the irregular shape of longleaf pine tree crowns likely further reduces tree detection accuracy compared to most other conifer species with more regular conical crowns.

Imputing Forest Attributes at Tree Level

In this study, we used an individual tree detection and crown delineation approach to compute HMAX and CA, which were subsequently employed as predictors to estimate tree-level metrics such as V and BA in a modeling framework (RF *k*-NN imputation). This is the first study to detect individual trees and model tree-level attributes using such an approach in longleaf pine forest.

In the modeling process, before building the tree-level RF *k*-NN imputation model, it was necessary to match individual trees detected from the LiDAR-derived CHM with the associated reference trees measured in the test plots. The rSTree was able to match up 48.0% of all reference trees. Most of the missed trees occurred in test plots with COV conditions over 70%. However, even though an ideal situation (i.e., matching all the LiDAR and reference trees) was not achieved, the rStree algorithm proposed herein is still appropriate for tree matching when GPS errors in the field-based stem map are an issue.

Error in estimating Ht, BA, and V came disproportionately from young trees, although these comprised only 1.9% of the total number of stems. Additional error could be attributed to the 1-year difference between the LiDAR acquisitions (2008)

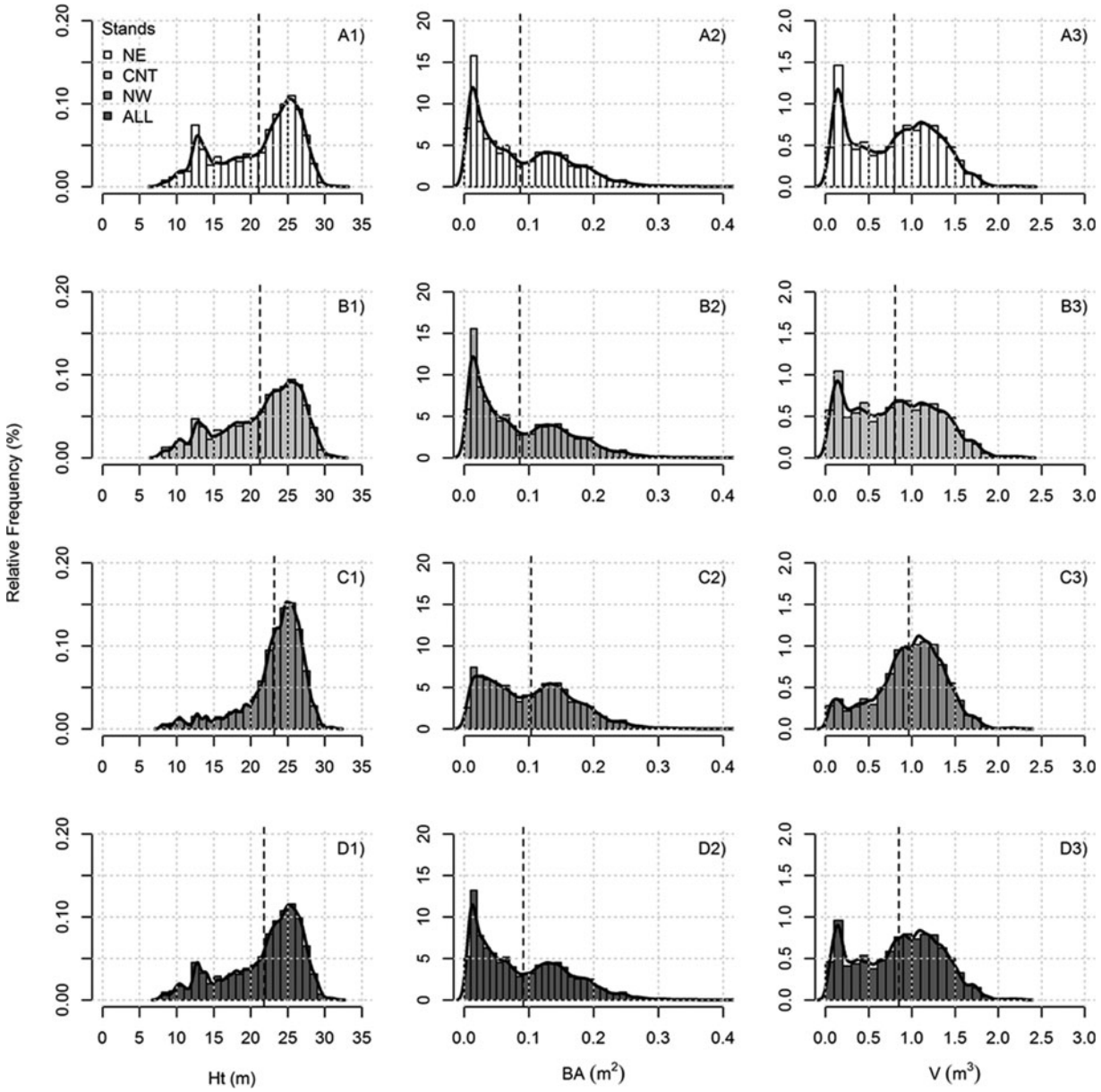

FIG. 11. Distribution of imputed tree attributes (Ht, BA, and V) across the 3 stands in the study area. The numbers from 1 to 3 represent the attributes Ht, BA, and V, respectively. The letters from (A) to (D) represent the NE, CNT, and NW, and all stands, respectively. The black line represents a fitted distribution and the dashed vertical line represents the mean.

and field measurements (2009). Nevertheless, the accuracies of the RF *k*-NN imputation model for imputing Ht and V were satisfactory, with RMSD in the cross-validation ranging from 2.96% to 8.19%, clearly surpassing the stated goal of less than 15%. However, the adjusted model was not able to accurately model BA. However, the primary contributor to the high BA estimation error is that the height–diameter allometry for longleaf pine breaks down after reaching a diameter of ∼25 cm, when height growth asymptotes at ∼25 m (Gonzalez-Benecke et al. 2014). The addition of crown-dimension attributes to a biometric model can help, but in this study it did not explain much BA variance.

The use of airborne LiDAR to retrieve forest attributes such as Ht, V, and BA at tree level has been not widely studied, however, some previous studies have shown the great potential of this technology to provide it. For example, Maltamo et al. (2009), using LiDAR-based metrics and *k*-Most Similar Neighbor (*k*-MSN) imputation for predicting tree-level characteristics from a reference dataset comprising 133 trees, reported relative RMSEs of 1.95%, 5.6%, and 11.0% for the Ht, DBH,

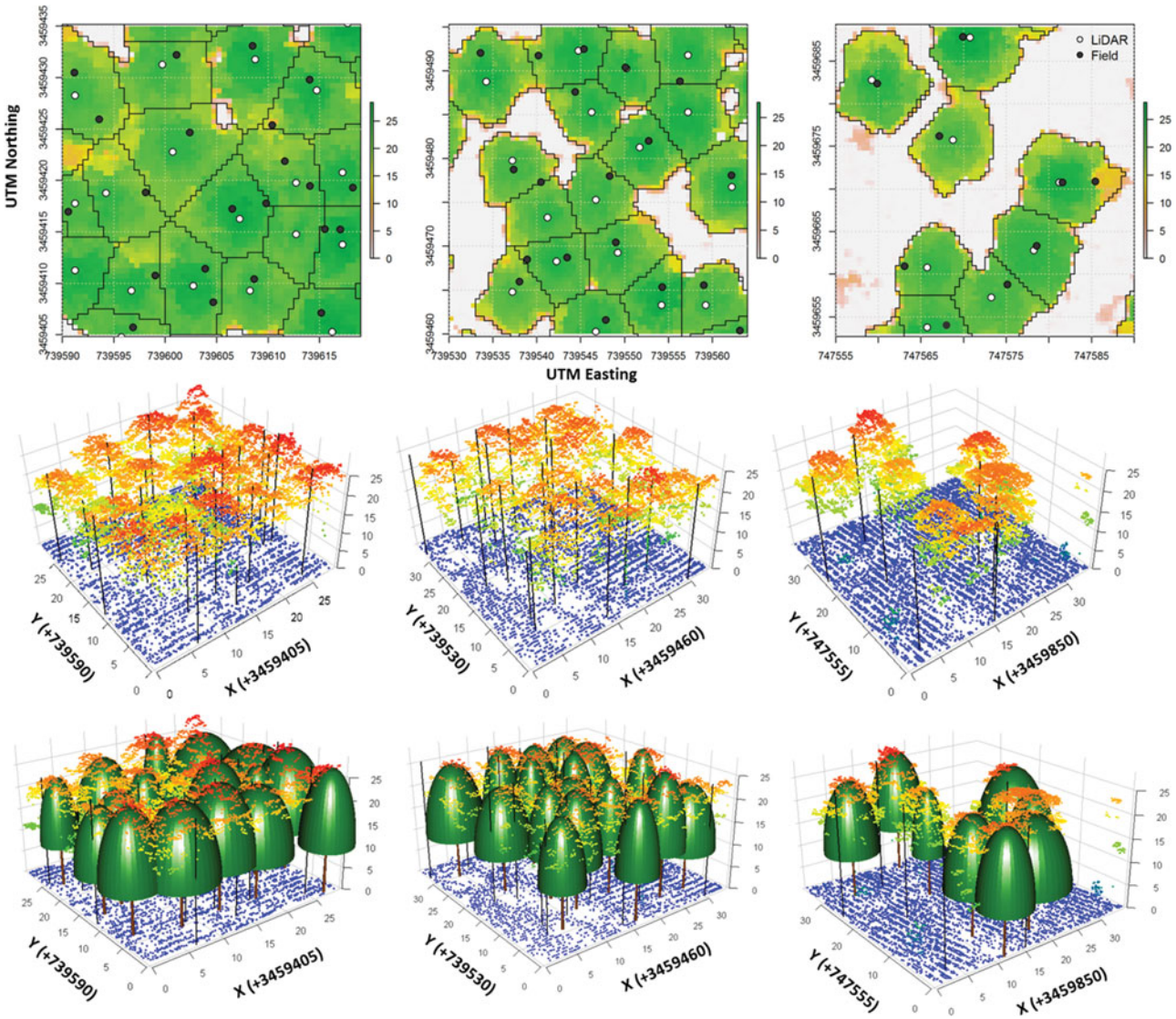

FIG. 12. Illustration of individual tree detection and crown delineation under different COV conditions. (1) COV = 90.96%; COV = 76.79%, and (3) COV = 58.66%. (A) 2D visualization of the tree location and crown delineation over the CHM. (B) 3D visualization of the LiDAR point cloud and reference trees measured in the field. (C) 3D visualization of the LiDAR virtual forest, and the reference tree locations.

Q10

and V attributes estimation in 14 Scots pine (*Pinus sylvestris* L.) plots located in the Koli National Park in North Karelia, eastern Finland. Vauhkonen et al. (2010), working in mixed conifer mixed forest dominated mostly by Scots pine and Norway spruce (*Picea abies* L. Karst.) in southern of Finland, employed *k*-MSN and RF imputation methods simultaneously for estimating stem dimensions using LiDAR-based variables, and reported relative RMSEs of 3%, 13% and 31%, for Ht, DBH, and V, respectively. Vastaranta et al. (2014) using a multisource single-tree inventory (MS-STI) in a broad mixture of forest stands located in Evo, Finland, reported RMSEs ranging from 4.2% to 5.3%, from 10.9% to 19.9% and from 28.7% to 43.5%, for Ht, DBH, and saw log volume, respectively. Our accuracies were not higher than those reports in Maltamo et al. (2009) and Vauhkonen et al. (2010). However, it is difficult to compare these results with ours owing to methodological and site differences.

Lindberg and Hollaus (2012) reported estimates of individual tree BA that were more accurate based on the regression models than those derived from identifying tree tops from local maxima in the CHM in hemi-boreal forest in the southwest of Sweden. Furthermore, Vauhkonen et al. (2010) reported that the variation in RMSEs of 11%–15% for individual-tree BA estimation was due to the type of method (*k*-MSN or RF), value of *k*, and

the set of predictor variables applied in the modeling process. In another study, also in Evo, Finland, Kankare et al. (2015) verified that the DBH accuracy was inversely proportional to tree density, where DBH accuracy decreased when tree density increased.

Our BA results might be improved by optimizing k or adding more individual tree metrics as predictors, such as canopy volume (Chen et al. 2007, Vauhkonen et al. 2010). Even though it is time consuming, individual tree segmentation directly from the LiDAR point cloud methods as presented by Reitberger et al. (2009), Ferraz et al. (2012) and Yao et al. (2013) are considered alternatives to increase the number of individual-tree metrics to be derived from the LiDAR point cloud data, as can be accomplished with the rLiDAR package (Silva 2015). We have tested the rLiDAR algorithms for individual-tree detection and crown delineation on a CHM derived from airborne LiDAR at plot and stand levels; the rLiDAR package is not designed to ingest large LiDAR datasets, due to inherent memory limitations of R compared to specialized LiDAR processing software such as FUSION/LDV and LAStools.

Stand-Level Forest Attributes Characterization

The longleaf pine forest attributes estimates reported in this study represent useful information for the study and management of the longleaf pine forest at the Ichauway site. The spatially detailed information such as the number, location, spacing, size, Ht, BA, and V distribution of individual trees as available in map form (not shown) helps managers achieve greater management and conservation efficiency. Forestry studies often produce estimates of the stand-level forest attributes and how they change over time (Gonzalez-Benecke et al. 2014). Therefore, the distributions of the structural forest attributes reported previously in Figure 11 are relevant for forest planning and assessments of economic value.

CONCLUSIONS

In this study, we investigated the use of LiDAR and RF k-NN imputation for individual tree detection and forest attributes modeling in longleaf pine forest. Overall, our method detects individual trees with high accuracy in areas with $< 70\%$ COV. The precision and accuracy of LiDAR in retrieving Ht and V parameters at an individual-tree level using the framework presented was clearly demonstrated through a relative RMSE and BIAS less than 15%. Even though the desired accuracy of BA was not fully attained, the framework presented herein can serve as a useful methodology, and the result will ultimately support further study and management of longleaf pine forest ecosystems in the study area. We hope that the promising results for individual-tree-level forest-attribute modeling in this study will stimulate further research and applications not just in longleaf pine but other forest types.

ACKNOWLEDGMENTS

We thank Nicholas L. Crookston and three anonymous reviewers for their helpful suggestions on an earlier draft of the manuscript.

FUNDING

This research was funded primarily from the US Department of Defense Strategic Environmental Research and Development Program (#RC-2243). Partial funding for this work was also provided through a PhD scholarship from the National Counsel of Technological and Scientific Development – CNPq via the Brazilian Science without Borders program (249802/2013-9) and the USDA Forest Service Rocky Mountain Research Station.

REFERENCES

Aurenhammer, F., and Klein, R. 1999. "Voronoi diagrams." In *Handbook on Computational Geometry*, edited by J.R. Sack and G. Urrutia, pp. 201–290. Amsterdam: Elsevier.

Breidenbach, J., Næsset, E., Lien, V., Gobakken, T., and Solberg, S. 2010. "Prediction of species specific forest inventory attributes using a nonparametric semi-individual tree crown approach based on fused airborne laser scanning and multispectral data." *Remote Sensing of Environment*, Vol. 114: pp. 911–924.

Breiman, L. 2001. "Random forest." *Machine Learning*, Vol. 45(No. 1): pp. 5–32.

Brockway, D.G., Outcalt, K.W., Tomczak, D.J., and Johnson, E.E. 2005. *Restoration of Longleaf Pine Ecosystems*. Report No. 83. Southern Research Station, Asheville, NC, USA: US Department of Agriculture, Forest Service.

Crookston, N.L., and Finley, A.O. 2008. yaImpute: An R package for kNN imputation. *Journal of Statistical Software*, Vol. 23: pp. 1–16.

Chen, Q., Baldocchi, D., Gong, P., and Kelly, M. 2006. "Isolating individual trees in a savanna woodland using small footprint LiDAR data." *Photogrammetric Engineering & Remote Sensing*, Vol. 72(No. 8): pp. 923–932.

Chen, Q., Gong, P., Baldocchi, D., and Tian, Y.Q. 2007. "Estimating basal area and stem volume for individual trees from LiDAR data." *Photogrammetric Engineering & Remote Sensing*, Vol. 73(No. 12): pp. 1355–1365.

Christensen, N.L. 1981. "Fire regimes in south-eastern ecosystems." In *Fire Regimes and Ecosystem Properties: Proceedings of the Conference. General Technical*. Report No. 26. edited by H.A. Mooney, T.M. Bonnicksen, J.R. Christensen, L. Norman, J.E. Lotan, and W.A. Reiners. Washington, D.: USDA Forest Service.

Dobbs Jr., R.H. 2011. *Environmental State of the State Longleaf Pine Ecosystem. Report No.1*. Atlanta, GA: R. Howard Dobbs Jr. Foundation.

Duncanson, L.I., Cook, B.D., Hurtt, G.C., and Dubayah, R.O. 2014. "An efficient, multi-layered crown delineation algorithm for mapping individual tree structure across multiple ecosystems." *Remote Sensing of Environment*, Vol. 154: pp. 378–386.

Duncanson, L.I., Dubayah, R.O., Cook, B.D., Rosette, J., and Parker, G. 2015. "The importance of spatial detail: Assessing the utility of individual crown information and scaling approaches for Lidar-based biomass density estimation." *Remote Sensing of Environment*, Vol. 168: pp. 102–12.

Falkowski, M.J., Smith, A.M.S., Gessler, P., Hudak, A.T., Vierling, L.A. and Evans, J.S. 2008. "The influence of conifer forest canopy cover on the accuracy of two individual tree measurement algorithms using LiDAR data." *Canadian Journal of Remote Sensing*, Vol. 34(No. 2): pp. S1–S13.

Falkowski, M.J., Evans, J.S., Martinuzzi, S., Gessler, P.E., and Hudak, A.T. 2009. "Characterizing forest succession with LiDAR data: An evaluation for the Inland Northwest, USA." *Remote Sensing of Environment*, Vol.113 (No. 5): pp. 946–956.

Falkowski, M.J., Hudak, A.T., Crookston, N.L., Gessler, P.E., Uebler, E.H., and Smith, A.M.S. 2010. "Nearest neighbor imputation approach incorporating LiDAR data." *Canadian Journal of Forest Research*, Vol. 40(No. 2): pp. 184–199.

Fekety, P.A, Falkowski, M.J., and Hudak, A.T. 2015. "Temporal transferability of LiDAR-based imputation of forest inventory attributes." *Canadian Journal of Forest Research*, Vol. 45(No. 4): pp. 422–435.

Ferraz, A., Bretar, F., Jacquemoud, S., Gonçalves, G., Pereira, L., Tomé, M., and Soares, P. 2012. "3-D mapping of a multi-layered Mediterranean forest using ALS data." *Remote Sensing of Environment*, Vol. 121: pp. 210–23.

Franklin, R.M. 2008. *Stewardship of Long Leaf Pine Forests: A Guide for Landowners. Report No. 2*. Clemson, SC, USA: Clemson University Cooperative Extension Service.

Frost, C. 2006. "History and future of the longleaf pine ecosystem." In *The Longleaf Pine Ecosystem: Ecology, Silviculture, and Restoration*, edited by S. Jose, E.J. Jokela, and D.L. Miller, pp. 9–48. New York: Springer Science & Business Media.

Gaveau, D.L., and Hill, R.A. 2003. "Quantifying canopy height underestimation by laser pulse penetration in small-footprint airborne laser scanning data." *Canadian Journal of Remote Sensing*, Vol. 29: pp. 650–657.

Gobakken, T., and Næsset, E. 2004. Estimation of diameter and basal area distributions in coniferous forest by means of Airborne Laser Scanner Data. *Scandinavian Journal of Forest Research*, Vol. 19(No. 6): pp. 529–542.

Goetz, S., Steinberg, D., Dubayah, R., and Blair, B. 2007. "Laser remote sensing of canopy habitat heterogeneity as a predictor of bird species richness in an Eastern Temperate forest, USA." *Remote Sensing of Environment*, Vol. 108(No. 3): pp. 254–263.

Gonzalez-Benecke, C.A., Gezan, S.A., Samuelson, L.J., Cropper, W.P., Leduc, D.L., and Martin, T.A. 2014. "Estimating *Pinus palustris* tree diameter and stem volume from tree height, crown area and stand-level parameters." *Journal of Forestry Research*, Vol. 25(No. 1): pp. 43–52.

Goutte, C., and Gaussier, E. 2005. "A probabilistic interpretation of precision, recall and F-score, with implication for evaluation." *Advances in Information Retrieval*, Vol. 3408: pp. 345–359.

Hansen, E.H., Gobakken, T., Bollandsås, O.M., Zahabu, E., and Næsset, E. 2015. "Modeling aboveground biomass in dense tropical submontane rainforest using airborne laser scanner data." *Remote Sensing*, Vol. 7(No. 1): pp. 788–807.

Hinsley, S.A., Hill, R.A., Gaveau, D.L.A., and Bellamy, P.E. 2002. "Quantifying woodland structure and habitat quality for birds using airborne laser scanning." *Functional Ecology*, Vol. 16(No. 6): pp. 851–857.

Hu, B., Li, J., Jing, L., and Judah, A. 2014. "Improving the efficiency and accuracy of individual tree crown delineation from high-density LiDAR data." *International Journal of Applied Earth Observation and Geoinformation*, Vol. 26: pp. 145–155.

Hudak, A.T., Crookston, N.L., Evans, J.S., Falkowski, M.J., Smith, A.M.S., and Gessler, P. 2006. "Regression modeling and mapping of coniferous forest basal area and tree density from discrete-return LiDAR and multispectral satellite data." *Canadian Journal of Remote Sensing*, Vol. 32(No. 2): pp. 126–38.

Hudak, A.T., Crookston, N.L., Evans, J.S, Hall, D.E., and Falkowski, M.J. 2008. "Nearest neighbor imputation of species-level, plot-scale forest structure attributes from LiDAR data." *Remote Sensing of Environment*, Vol. 112(No. 5): pp. 2232–2245.

Hudak, A.T., Evans, J.S., and Smith, A.M.S. 2009. "LiDAR utility for natural resource managers." *Remote Sensing*, Vol. 1(No. 4): pp. 934–951.

Hudak, A.T., Haren, A.T., Crookston, N.L., Liebermann, R.J., and Ohmann, J.L. 2014. "Imputing forest structure attributes from stand inventory and remotely sensed data in Western Oregon, USA." *Forest Science*, Vol. 60(No. 2): pp. 253–269.

Hudak, A.T., Strand, E.K., Vierling, L.A., Byrne, J.C., Eitel, J.U.H., Martinuzzi, S., and Falkowski, M.J. 2012. "Quantifying aboveground forest carbon pools and fluxes from repeat LiDAR surveys." *Remote Sensing of Environment*, Vol. 123: pp. 25–40.

Hyyppä, J., Kelle, O., Lehikoinen, M., and Inkinen, M., 2001. "A segmentation-based method to retrieve stem volume estimates from 3-D tree height models produced by laser scanners." *IEEE Transactions on Geoscience and Remote Sensing*, Vol. 39(No. 5): pp. 969–975.

Isenburg, M. 2015. *LAStools—Efficient Tools for LiDAR Processing*, accessed October 3, 2015.<lastools.org>

Jing, L., Hu, B., Li, J., and Noland, T., 2012. "Automated delineation of individual tree crowns from LiDAR data by multi-scale analysis and segmentation." *Photogrammetric Engineering & Remote Sensing*, Vol. 78(No. 12): pp. 1275–1284.

Jing, L., Hu, B., Li, H., Li, J., and Noland, T. 2014. "Automated individual tree crown delineation from LiDAR data using morphological techniques." *IOP Conference Series: Earth and Environmental Science*, Vol. 17: pp. 121–152.

Kankare, V., Liang, X., Vastaranta, M., Yu. X., Holopainen, M., and Hyppä. J. 2015. "Diameter distribution estimation with laser scanning based multisource single tree inventory." *ISPRS Journal of Photogrammetry and Remote Sensing*, Vol. 108: pp. 161–171.

Kirkman, L.K., Goebel, P.C., Palik, B.J. and West, L.T. 2004. "Predicting plant species diversity in a longleaf pine landscape."*Ecoscience*, Vol. 11(No. 1): pp. 80–93.

Khosravipour, A., Skidmore, A.K., Isenburg, M., Wang, T., and Hussin, Y.A. 2014. "Generating pit-free canopy height models from airborne LiDAR." *Photogrammetric Engineering & Remote Sensing*, Vol. 80(No. 9): pp. 863–872.

Kraus, K., and Pfeifer, N. 1998. "Determination of terrain models in wooded areas with airborne laser scanner data." *ISPRS Journal of Photogrammetry & Remote Sensing*, Vol. 53: pp. 193–203.

Koch, B., Heyder, U., and Weinacker, H. 2006. "Detection of individual tree crowns in airborne LiDAR data." *Photogrammetric Engineering & Remote Sensing*, Vol. 72(No. 4): p. 357.

Lähivaara, T., Seppänen, A., Kaipio, J.P., Vauhkonen, J., Korhonen, L., Tokola, T., and Maltamo, M. 2014. "Bayesian approach to tree detection based on airborne laser scanning data." *IEEE Transactions on Geoscience and Remote Sensing*, Vol. 52(No. 5): pp. 2690–2699.

Landers, J.L., Van Lear, D.H., and Boyer, W.D. 1995. "The longleaf pine forests of the Southeast: requiem or renaissance?" *Journal of Forestry*. Vol. 93(No. 11): pp. 39–44.

Leckie, D., Gougeon, F., Hill, D., Quinn, R., Armstrong, L., and Shreenan, R. 2003. "Combined high-density LiDAR and multispectral imagery for individual tree crown analysis." *Canadian Journal of Remote Sensing*, Vol. 29(No. 5): pp. 633–649.

Li, W., Guo, Q., Jakubowski, M.K. and Kelly, M. 2012. "A new method for segmenting individual trees from the LiDAR point cloud." *Photogrammetric Engineering & Remote Sensing*, Vol. 78(No. 1): pp. 75–84.

Lindberg, E., and Hollaus, M. 2012. "Comparison of methods for estimation of stem volume, stem number and basal area from airborne laser scanning data in a hemi-boreal forest." *Remote Sensing*, Vol. 4(No. 4): pp. 1004–1023.

Loudermilk, E.L., Cropper Jr., P., Mitchell, R.J., and Lee, H. 2011. "Longleaf pine (*Pinus palustris*) and hardwood dynamics in a fire-maintained ecosystem: A simulation approach." *Ecological Modelling*, Vol. 222(No. 15): pp. 2733–2750.

Lucas, R., Lee, A., and Williams, M. 2005. "The role of LiDAR data in understanding the relation between forest structure and SAR imagery." *International Geoscience and Remote Sensing Symposium (IGARSS)*, Vol. 3: pp. 2101–2104.

Maltamo, M., Mustonen, K., Hyyppä, J., Pitkänen, J., and Yu, X. 2004. "The accuracy of estimating individual tree variables with airborne laser scanning in a Boreal Nature Reserve." *Canadian Journal of Forest Research*, Vol. 34(No. 9): pp. 1791–1801.

Maltamo, M., Peuhkurinen, J., Malinen, J., Vauhkonen, J., Packalén, P., and Tokola. P. 2009. "Predicting tree attributes and quality characteristics of scots pine using airborne laser scanning data." *Silva Fennica*, Vol. 43(No. 3): pp. 507–521.

McGauchey, R.J. 2015. *FUSION/LDV: Software for LiDAR Data Analysis and Visualization*. Forest Service Pacific Northwest Research Station USDA, Seattle, accessed Oct. 15 2015, <http://http://forsys.cfr.washington.edu/fusion/ FUSION_manual.pdf>.

McRoberts, R.E., Næsset, E., and Gobakken, T. 2015. "Optimizing the k-nearest neighbor technique for estimating forest aboveground biomass using airborne laser scanning data." *Remote Sensing of Environment*, Vol.163: pp. 13–22.

Means, J., and Acker, S. 2000. "Predicting forest stand characteristics with airborne scanning LiDAR." *Photogrammetric Engineering & Remote Sensing*, Vol. 66(No. 11): pp. 1367–1371.

Mutlu, M., Popescu, S.C., Curt, S., and Spencer, T. 2008. "Mapping surface fuel models using LiDAR and multispectral data fusion for fire behavior." *Remote Sensing of Environment*, Vol. 112(No. 1): pp. 274–285.

Næsset, E. 1997. "Determination of mean tree height of forest stands using airborne laser scanner data." *ISPRS Journal of Photogrammetry and Remote Sensing*, Vol. 52(No. 2): pp. 49–56.

Næsset, E., and Bjerknes, K.O. 2001. "Estimating tree heights and number of stems in young forest stands using airborne laser scanner data." *Remote Sensing of Environment*, Vol. 78(No. 3): pp. 328–340.

Næsset, E., and Økland, T. 2002. "Estimating tree height and tree crown properties using airborne scanning laser in a boreal nature reserve." *Remote Sensing of Environment*, Vol. 79(No. 1): pp. 105–115.

Nelson, M.D., Healey, S.P., Moser, W.K., Maser, J.G., and Cohen, W.B. 2011. "Consistency of forest presence and biomass predictions modeled across overlapping spatial and temporal extents." *Mathematical and Computational Forestry & Natural Resource Science*, Vol. 3(No. 2): pp. 102–113.

Nelson, R., Krabill, W., and Tonelli, J. 1988. "Estimating forest biomass and volume using airborne laser data." *Remote Sensing of Environment*, Vol. 24(No. 2): pp. 247–267.

Nilsson M. 1996. "Estimation of tree heights and stand volume using an airborne LiDAR system." *Remote Sensing of Environment*, Vol. 56: pp. 1–7.

Oswalt, C.M., Cooper, J.A., Brockway, D.G., Brooks, H.W., Walker, J.L., Connor, K.F., Oswalt, S.N., and Conner, R.C. 2012. *History and Current Condition of Longleaf Pine in the Southern United States. Report No. 166*. Southern Research Station, Asheville, NC, USA. > US Department of Agriculture Forest Service.

Palik, B., Mitchell, R.J., Pecot, S., Battaglia, M., and Pu, M. 2003. "Spatial distribution of overstory retention influences resources and growth of longleaf pine seedlings." *Ecological Applications*, Vol. 13: pp. 674–686.

Pang, Y., Lefsky, M., Andersen, H.E., Miller, M.E., Sherrill, K., 2008. "Validation of the ICEsat vegetation product using crown-area-weighted mean height derived using crown delineation with discrete return LiDAR data." *Canadian Journal of Remote Sensing. Vol.* 34(No. 2): pp. 471–484.

Popescu, S.C. 2007. "Estimating biomass of individual pine trees using airborne LiDAR." *Biomass and Bioenergy*, Vol. 31(No. 9): pp. 646–655.

Popescu, S.C., Wynne, R.H., and Nelson, R.F. 2003. "Measuring individual tree crown diameter with LiDAR and assessing its influence on estimating forest volume and biomass." *Canadian Journal of Remote Sensing*, Vol. 29(No. 5): pp. 564–577.

R Core Team. 2015. *R: A Language and Environment for Statistical Computing*. R Foundation for Statistical Computing, Vienna, Austria, accessed Oct. 15 2015, <http://www.R-project.org≥.

Racine, E.B., Coops, N.C., St-Onge, B., and Begin, J. 2014. "Estimating forest stand age from LiDAR-derived predictors and nearest neighbor imputation." *Forest Science*, Vol. 60(No. 1): pp. 128–136.

Reitberger, J., Schnörr, C.L., Krzystek, P., and Stilla, U. 2009. "3D segmentation of single trees exploiting full waveform LiDAR data." *ISPRS Journal of Photogrammetry and Remote Sensing*, Vol. 64(No. 6): pp. 561–574.

Robinson, A.P., Duursma, R.A., and Marshall, J.D. 2005. "A regression-based equivalence test for model validation: shifting the burden of proof." *Tree Physiology*, Vol. 25: pp. 903–913.

Robinson, A. 2015. *Equivalence: Provides Tests and Graphics for Assessing Tests of Equivalence*, version 0.7.0, accessed Oct. 15 2015, <https://cran.r-project.org/web/packages/ equivalence/>.

Rombouts, J., Melville, G., Kathuria, A., Rawley, B., and Stone, C. 2015. *Operational Deployment of LiDAR Derived Information into Softwood Resource Systems. Report No. 61*. Melbourne, Australia: Forest & Wood Products Australia.

Saarinen, N., Vastaranta, M., Kankare, V., Tanhuanpää, T., Holopainen, M., Hyyppä, J., and Hyyppä, H. 2014. "Urban tree attribute update using multisource single tree inventory." *Forests*, Vol. 5(No. 5): pp. 1032–052.

Saremi, H., Kumar, L., Stone, C., Melville, G., and Turner, R. 2014. "Sub-compartment variation in tree height, stem diameter and stocking in a *Pinus radiata* D. Don plantation examined using airborne LiDAR data." *Remote Sensing*, Vol. 6(No. 8): pp. 7592–7609.

Shamsoddini, A., Turner, R., and Trinder, J.C. 2013. "Improving LiDAR-based forest structure mapping with crown-level pit removal." *Journal of Spatial Science*, Vol. 58: pp. 29–51.

Silva, C.A., Crookston, N.L., Hudak, A.T., and Vierling, L.A. 2015. *rLiDAR: An R package for reading, processing and visualizing LiDAR (Light Detection and Ranging) data, version 0.1*, accessed Oct. 15 2015, < http://cran.r-project.org/web/packages/rLiDAR/index.html>.

Silva, C.A., Klauberg, C., Carvalho, S.P.C., Hudak, A.T., and Rodriguez, L.C.E. 2014. "Mapping aboveground carbon stocks using LiDAR data in *Eucalyptus* spp. plantations in the state of São Paulo, Brazil." *Sciencia Forestalis*, Vol. 42: pp. 591–604.

Smith, A.M.S., Falkowskie, M.J., Hudak, A.T., Evans, J.S., Robinson, A.P., and Steele, C.M. 2009. "A cross-comparison of field, spectral, and LiDAR estimates of forest canopy cover." *Canadian Journal of Remote Sensing*, Vol 35(No. 5): pp. 447–459.

Sokolova, M., Japkowicz, N., and Szpakowicz, S. 2006. "Beyond accuracy, F-score and ROC: A family of discriminant measures for performance evaluation." In *Advances in Artificial Intelligence*, edited by A. Sattar and B.H. Kang, pp. 1015–102. Berlin, Heidelberg: Springer.

Solberg, S., Næsset, E., and Bollandsas, O.M., 2006. "Single tree segmentation using airborne laser scanner data in a structurally heterogeneous spruce forest." *Photogrammetry Engineering and Remote Sensing*, Vol. 72(No. 12): pp.1369–1378.

Stage, A.R., and Crookston, N.L. 2007. "Partitioning error components for accuracy-assessment of near neighbor methods of imputation." *Forest Science*, Vol. 53(No. 1): pp. 62–72.

Vastaranta, M., Saarinen, N., Kankare, V., Holopainen, M., Kaartinen, H., Hyyppä, J., Hyyppä. 2015. "Multisource single tree inventory in prediction of tree quality variables and logging recoveries." *Remote Sensing*, Vol. 6(No. 4): pp. 3475–3491.

Vauhkonen, J., Ene, L., Gupta, L., Heinzel, L., Holmgren, J., Pitkãnen, J., Solberg, J.P.S., et al. 2012. "Comparative testing of single-tree detection algorithms under different types of forest." *Forestry*, Vol. 85(No. 1): pp. 27–40.

Vauhkonen, J., Korpela, I., Maltamo, M., and Timo Tokola. 2010. "Imputation of single-tree attributes using airborne laser scanning-based height, intensity, and alpha shape metrics." *Remote Sensing of Environment*, Vol. 114(No. 6): pp. 1263–76.

Vega, C., Hamrouni, A., Mokhtari, S.E., Morel, J., Bock, J., Renaud, J.P., Bouvier, M., and Durrieu, B. 2014. "PTrees: A point-based approach to forest tree extraction from LiDAR data." *International Journal of Applied Earth Observation and Geoinformation*, Vol. 33: pp. 98–108.

Vierling, K.T., Vierling, L.A., Gould, W.A., Martinuzzi, S., and Clawges, R.M. 2008. "Lidar: Shedding new light on habitat characterization and modeling." *Frontiers in Ecology and the Environment*, Vol. 6(No. 2): pp. 90–98.

Waske, B., Benediktsson, J.A., and Sveinsson, J.R. 2012. "Random forest classification of remote sensing data." In *Signal and Image Processing for Remote Sensing*, edited by C.H. Chen, pp. 365–374. Abingdon, UK: CRC Press, Taylor & Francis Group.

Weinacker, H., Koch, B., Heyder, U., and Weinacker, R. 2004. "Development of filtering, segmentation and modelling modules for LIDAR and multispectral data as a fundamental of an automatic forest inventory system." *Photogrammetry, Remote Sensing and Spatial Information Sciences*. *Vol.* 36(Part 8): pp. 50–55.

Wing, M.G., Eklund, A., Sessions, J., and Karsky, R. 2008. "Horizontal measurement performance of five mapping-grade GPS receiver configurations in several forested settings." *Western Journal of Applied Forestry*, Vol. 23(No. 3): pp. 166–171.

Wulder, M., Niemann, K.O., and Goodenough, D.G. 2000. "Local maximum filtering for the extraction of tree locations and basal area from high spatial resolution imagery." *Remote Sensing of Environment*, Vol. 73(No. 1): pp. 103–114.

Yao, W., Krzystek, P., and Heurich, M. 2013. "Enhanced detection of 3D individual trees in forested areas using airborne full-waveform LiDAR data by combining normalized cuts with spatial density clustering." *ISPRS Annals of Photogrammetry, Remote Sensing and Spatial Information Sciences*, Vol. II-5/W2: pp. 349–354.

Zimble, D.A., Evans, D.L., Carlson, G.C., Parker, R.C., Grado, S.C., and Gerard, P.D. 2003. Characterizing vertical forest structure using small-footprint airborne LiDAR. *Remote Sensing of Environment*, Vol. 87(No. 2–3): pp. 171–82.